Nuclear Inst. and Methods in Physics Research, A 878 (2018) 1–9

Contents lists available at ScienceDirect

Nuclear Inst. and Methods in Physics Research, A

journal homepage: www.elsevier.com/locate/nima

Radiation imaging with gaseous detectors

Fabio Sauli

CERN, Geneva, Switzerland

ARTICLE INFO

Keywords:
Radiation imaging
Gaseous detectors applications
Micro-pattern detectors

ABSTRACT

Modern position-sensitive fast gaseous detectors, developed primarily to satisfy the needs of particle physics experiments, have been tailored by many research groups for the use in other applied fields, owing to their main performances: high rate capability, sub-mm position resolution, large covered areas at moderate costs. Implemented with electronic or optical detection systems, the devices are successfully used to image various radiation fields: X-rays, low energy electrons, neutrons.

Contents

1. Introduction: evolution of gaseous detectors

Introduced in the late sixties, the Multiwire Proportional Chamber (MWPC [1]) represented a major progress in the field of fast, position-sensitive detectors and was swiftly and widely used in particle physics experimental setups [2]. Soon after their introduction, and with various modifications, MWPC devices were soon deployed in a variety of other applied research fields: medicine, biology, astrophysics [3]. While very successful in terms of performances, with rare exceptions wire-based detectors remain limited in use, mainly because of a fragile mechanical structure and of a modest space resolution determined by the wire distance.

A major progress in the field of gaseous detectors started with the development of the Micro-Strip Gas Chamber (MSGC [4]), where amplification and localization are performed on sets of thin metallic strips, etched on insulating substrates with industry-standard photolithographic processes. With anode strips pitch of few hundred microns, as compared to several mm for MWPC, MSGCs led to a substantial improvement in rate capability and localization accuracy [5]. Further work, however, exposed a serious problem of the devices: the tendency to develop damaging discharges in harsh operating conditions, such as those met in high-energy physics experiments [6]. Owing to the resulting limited reliability, the detectors were used only for a limited number of applications.

A new generation of devices, collectively named Micro-Pattern Gas detectors (MPGD) came to the rescue at the end of the eighties: the Micro-Mesh Gaseous Structure (Micromegas [7]), the Gas Electron Multiplier (GEM [8]), the Micro-Hole and Strip Plate (MHSP [9], the Micro-Pixel chamber [10] and many others demonstrated to have superior performances and higher reliability, and are widely used nowadays in particle physics experiments as well as in several other applied fields [11,12]. The present note describes examples of use of MPGDs in applications where their *imaging* characteristics, a direct or computer-mediated visual representations of radiation are of paramount relevance.

2. Imaging with electronic readout systems

As other gaseous devices, MPGDs exploit the release of ionization (electron-ion pairs) followed by a process of charge amplification, and are generally capable of achieving the large gains needed for detection of a wide field of radiation. Localization is achieved recording electronically the amplified charge profile on patterned electrodes, or,

E-mail address: fabio.sauli@cern.ch.

https://doi.org/10.1016/j.nima.2017.01.056
Received 24 August 2016; Received in revised form 21 November 2016; Accepted 24 January 2017
Available online 25 January 2017
0168-9002/

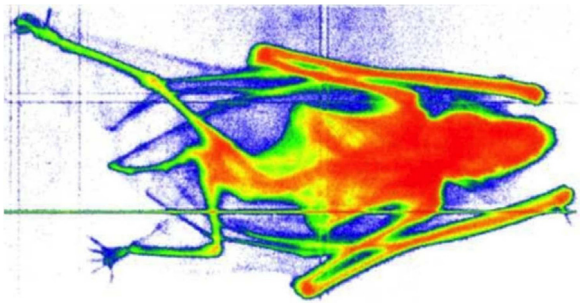

Fig. 1. 8 keV absorption radiography of a bat recorded with a two-dimensional GEM detector (image size: 7×3 cm^2) [14].

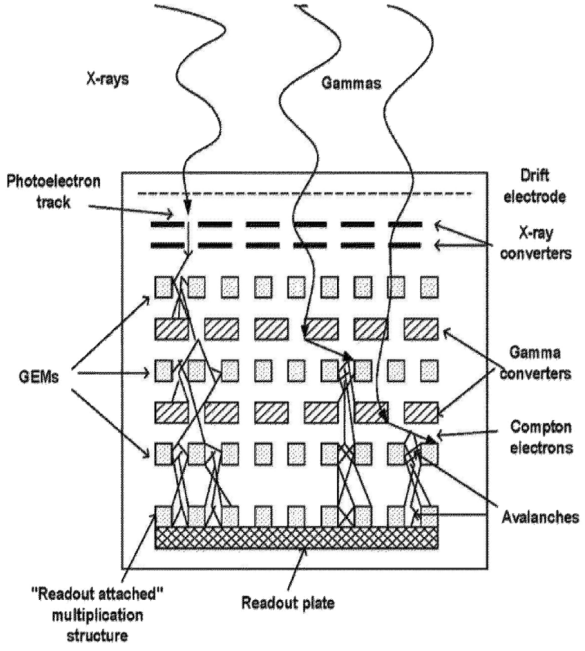

Fig. 2. Multi-GEM and converters structure designed for portal imaging of soft and hard gamma rays [16].

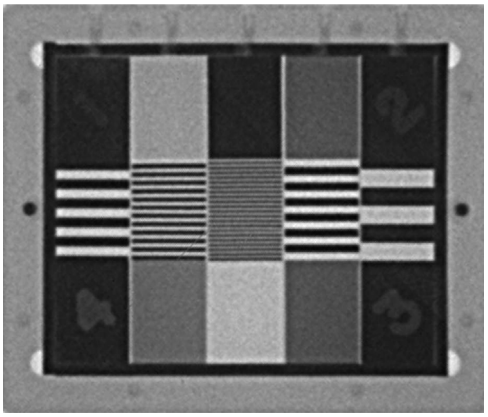

Fig. 3. 1.5 MeV radiography of a QC-3 phantom (courtesy C-RAD Imaging [18]).

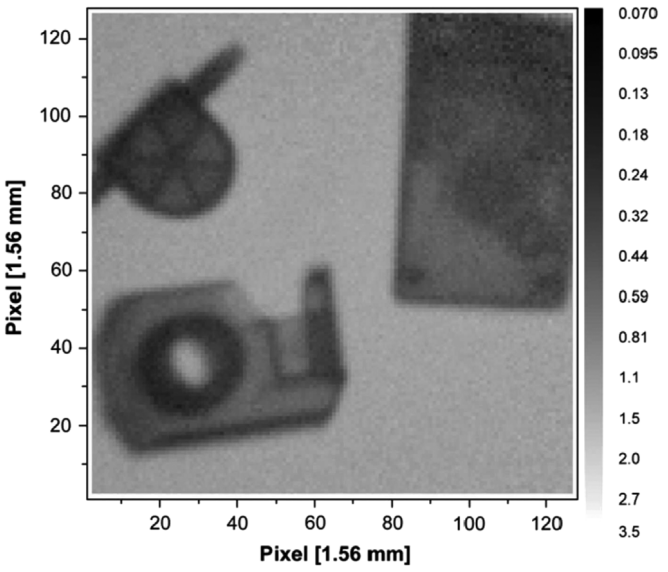

Fig. 4. Thermal neutron radiography recorded with CASCADE [19].

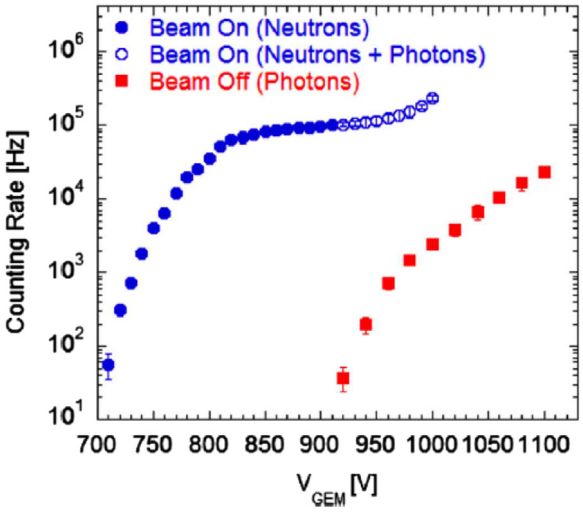

Fig. 5. Relative counting rates for neutrons and photons as a function of operating voltage of the b-GEM [20].

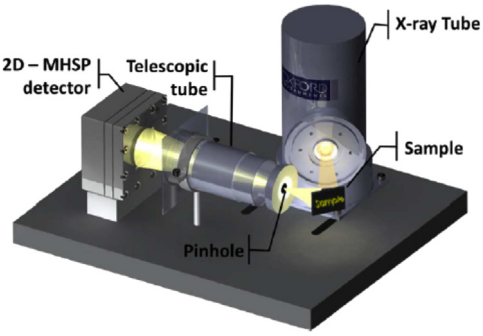

Fig. 6. MHSP-based EDXFR detector [21].

(as described in the next section) detecting the fluorescence induced by the impact of electrons with the gas molecules with optical sensors.

Owing to their conception, GEM-based devices are particularly versatile for a wide range of applications. The active electrode is a thin metal-clad insulating foil, pierced chemically or mechanically by a high-density of narrow holes. Application of a difference of potential between the two conductive sides induces the growth of electron-ion avalanches, initiated by the primary ionization; the amplified electron charge in the

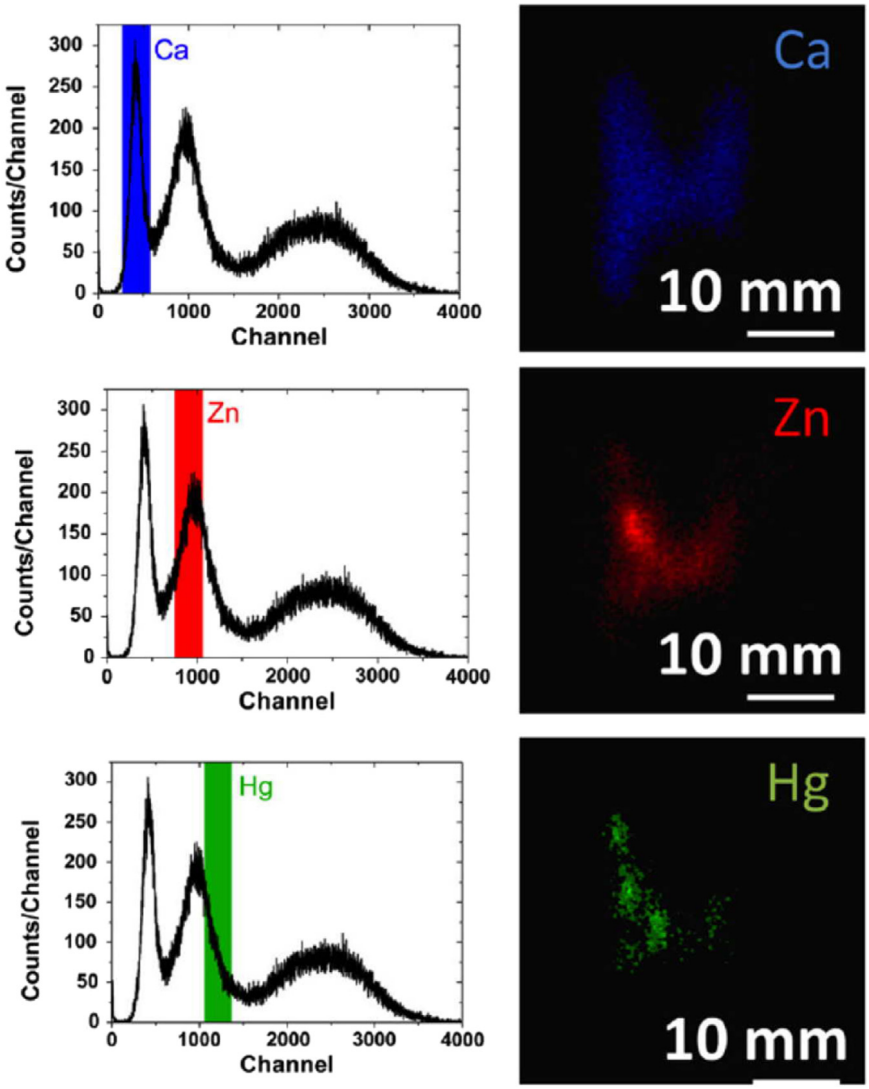

Fig. 7. Energy-resolved 2-D plots of the target in three adjacent X-ray energy regions [22].

front of the avalanches is then collected, or re-injected into a second GEM foil. This can be repeated several times, and permits reaching very high and stable gains. The last step in the process is a simple electron charge collection on the anode, that can be set at ground potential and patterned according to the needs.

Concurrently with the development of the detectors, several lines of readout electronics have been designed and produced to satisfy the experimental requirements [13]. In the most sophisticated models, they perform amplification and fast recording of the charge on each sensing electrode, strip or pad; owing to electron diffusion in the gas, a center-of-gravity calculation on the recorded charge profile permits to achieve localization accuracies much better than the strip's pitch. This is shown in Fig. 1, a two-dimensional digital radiography of a small mammal recorded with one of the early GEM devices; obtained exposing the object to an 8 keV X-ray beam, the image demonstrates the good contrast and sub-mm resolution achievable [14].

The detection efficiency of thin layers of gas is sufficiently high for soft X-rays; for higher energies however it becomes too low for most practical uses. Thin, high-Z metallic foils used as cathodes or deposited on the GEM electrodes convert a fraction of the incident flux in photoelectrons, emerging from the converter and ionizing the gas; for a Au-coated GEM electrode the efficiency is ~0.7% for gamma energies between 80 and 200 keV [15], and can be increased using multiple GEM-converter stacks. An example is shown in Fig. 2, optimized for the

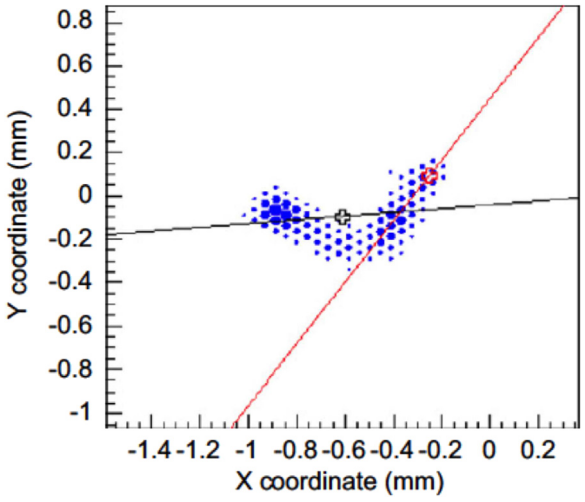

Fig. 8. 5.9 keV photoelectron track recorded with the GEM polarimeter [23].

detection of both soft and hard gamma rays, and used for deep tumor imaging; placed after the distal end of the patient, the device has been

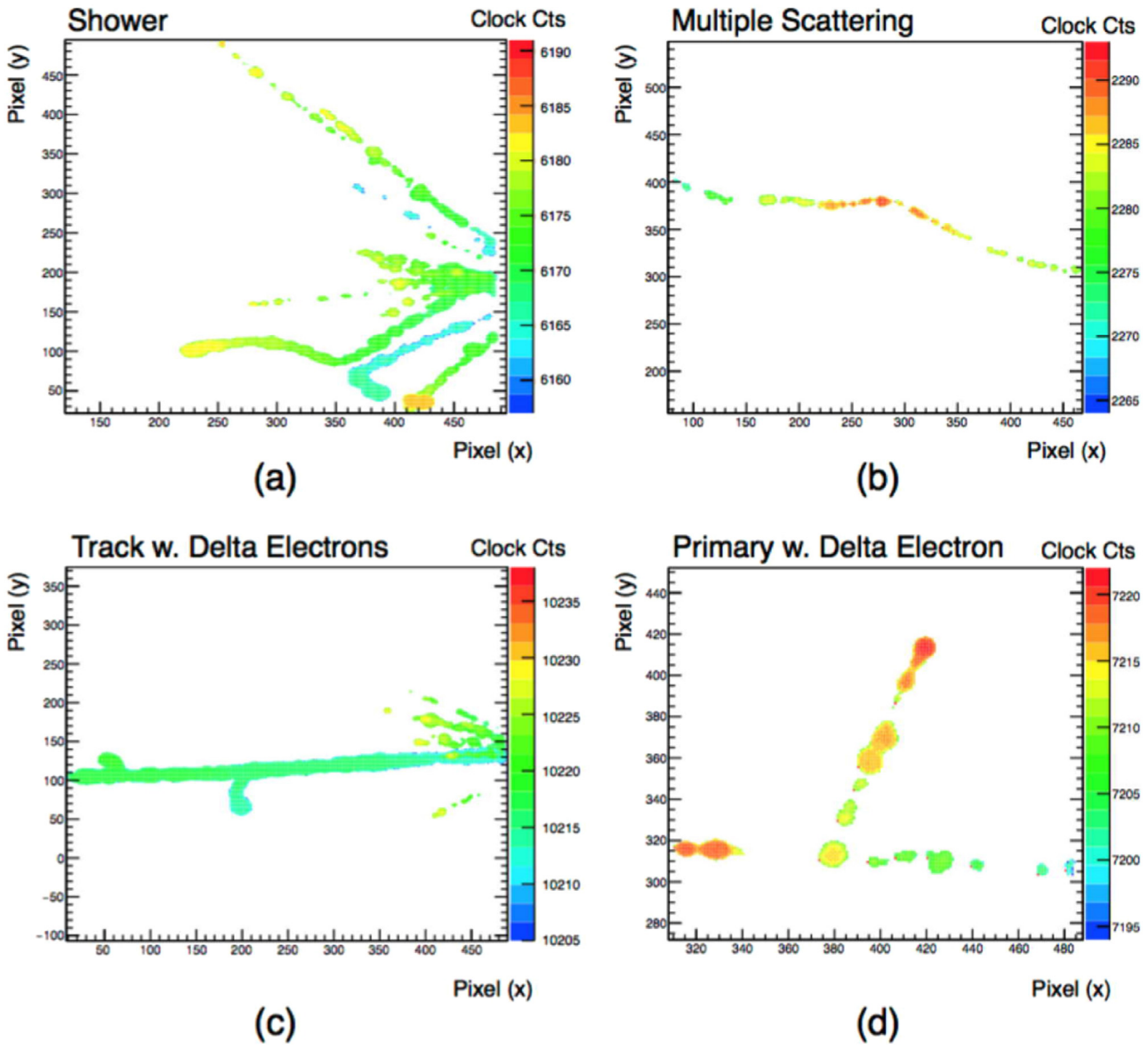

Fig. 9. Events recorded with the GEMPIX hybrid detector [26].

shown to efficiently perform on-line portal imaging [16]. To prevent being damaged by radiation, the electronics has to be removed from the direct beam and well screened [17].

Further refinements of the detector and associated electronics have led to the development of a commercial product, the GEMini portal imaging system, produced by the company C-RAD; the instrument has a GEM-based X-ray detector, recording the amplified charge on a 866×866 2-D pixel matrix at 450 μm pitch. Fig. 3 is a QC-3 phantom radiography recorded with the device with 1.5 MeV gammas [18].

Similar multi-GEM and converter structures have been developed for the detection and imaging neutrons. The detector CASCADE is a double-sided device with thin ^{10}B converters on the outer cathodes and GEM electrodes, with a common readout electrode in the middle. The device has an average thermal neutron detection efficiency of 50% at 15 Å and 1.7 mm resolution FWHM when operated at 2 bar; Fig. 4 is an example of thermal neutron radiography of common desk objects [19].

One of the peculiar features of the GEM-based neutron detectors is the very low sensitivity to intense gamma background, often present in spallation sources; Fig. 5 is a measurement of counting rate as a function of operating voltage for a triple-GEM detector with a cathode coated with 1 μm of boron carbide, the so-called b-GEM [20].

A field where the use of fast, accurate position-sensitive devices has received a lot of attention is the soft X-ray fluorescence analysis; with a simultaneous recording of the energy of the scattered photon, MPGD-based detectors permit to perform energy-dispersive fluorescence analysis (EDXRF) that permits the identification of the elemental constituents in samples. Using as readout pairs of delay lines connected on perpendicular strips on the anode, the authors of Ref. [21] have constructed and operated the rather compact instrument shown in Fig. 6.

Fig. 7 from the same reference is an example of elemental analysis of a composite target, with three images obtained selecting successive regions in the pulse height spectrum of the recorded fluorescence X-rays. Other applications include the mapping of the distribution of dental amalgams constituents in teeth and the elemental analysis of pigments used in ancient miniatures [22].

A far-fetched line of development is the direct coupling of a gaseous amplification structure, GEM or Micromegas, to a solid state pixel sensor, custom-designed or adapted from existing silicon devices. With pixel sizes of around 100 μm, the low capacitance coupled to the large gains achievable in the overlaying gas amplifier, hybrid devices can detect and image single electrons released in the gas. Fig. 8 is an example

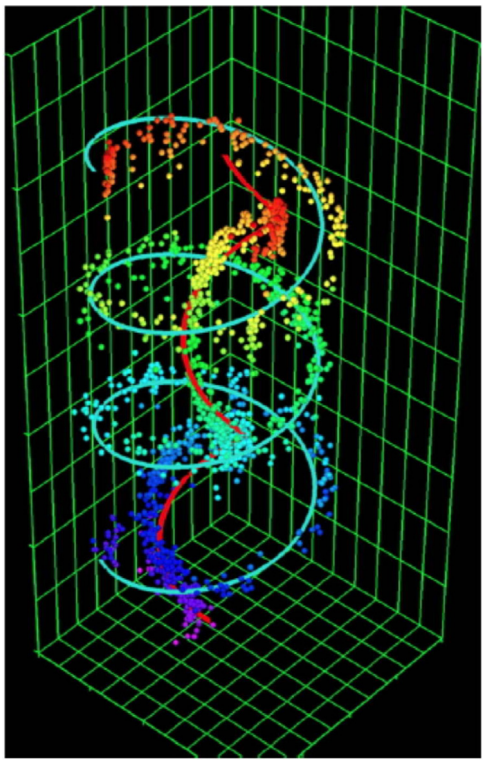

Fig. 10. Spiraling electron tracks recorded with the INGRID hybrid detector [28].

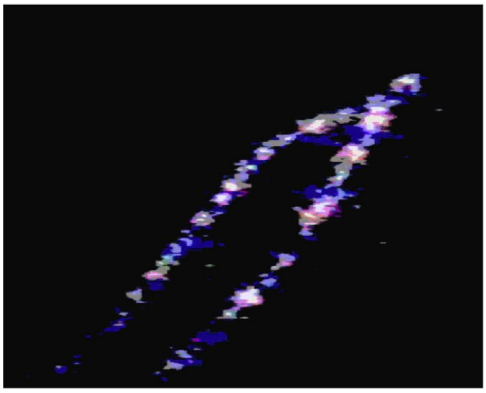

Fig. 11. Cosmic tracks detected with the imaging chamber [30].

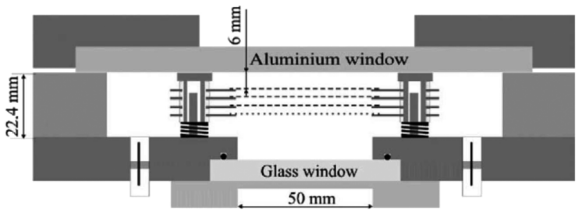

Fig. 12. Schematics of a Triple GEM designed for optical recording [32].

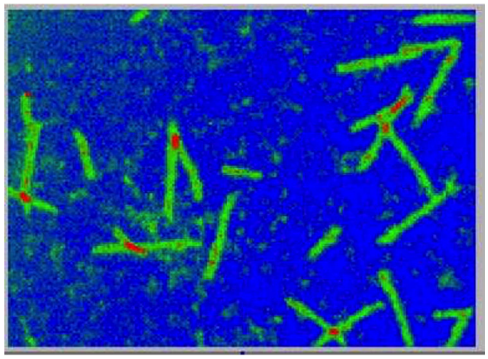

Fig. 13. Integral image of neutron interactions in ^{3}He-CF_4 [32].

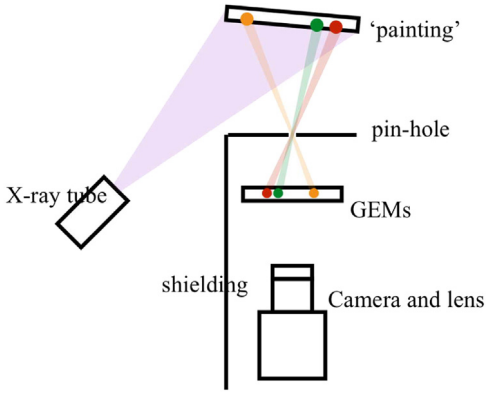

Fig. 14. Schematics of the pin-hole camera for fluorescence analysis [34].

of ionization trail recorded for a 5.9 keV photoelectron resulting from an X-ray interaction in the sensitive volume [23]; the size of each dot is proportional to the detected charge on a custom ASIC chip with a matrix of ~2000 hexagonal pixels at 80 μm pitch. The larger integral charge on one end of the trail corresponds to the Bragg peak; as shown by the reconstructed lines, the device permits to deduce the direction of emission, that depends on the photon polarization. Appropriately named X-ray polarimeter, the detector permits to determine the average polarization of stellar X-ray sources in astrophysics investigations. An improved version of the instrument has been built for deployment on board of a satellite of the European Space Agency telescope [24].

Developed as solid state detectors for medical applications, a line of large scale integrated chips (MEDIPIX and TIMEPIX [25]), stripped of their silicon pixels sensors, are particularly suitable for the realization of hybrid detectors. Named micro-TPCs, these devices perform tracking of high-multiplicity events with unprecedented resolution, as shown by Fig. 9, recorded with a triple GEM assembled over a TIMEPIX chip with a sensitive area of 7.3×6.9 mm^2 [26]. Used in a pinhole camera configuration, the detector has been used to record 2-D images of the soft X-ray emission of the laser production plasma [27].

The gaseous amplifying structure can be directly built over an existing solid state sensor exploiting silicon foundry technologies. Fig. 10 shows electron tracks spiraling in magnetic field, recorded with a Micromegas-like electrode built over the TIMEPIX chip, having ~66,000 square pixels 55 μm on the side, named INGRID [28].

While limited in size, hybrid detectors can be assembled side-to-side to cover larger sensitive areas.

3. Optical image recording

Concurrently with the creation of electron-ion pairs, photons are copiously emitted by the excited molecules in the avalanches, and can be exploited for detection. Energy and intensity of the emission depend on field and gas composition, a basic rule of thumb being that electrons and photons are produced in approximately equal amounts; however, most gases under avalanche condition fluoresce in the vacuum ultraviolet domain, difficult to detect due to self-absorption in the gas and in the windows.

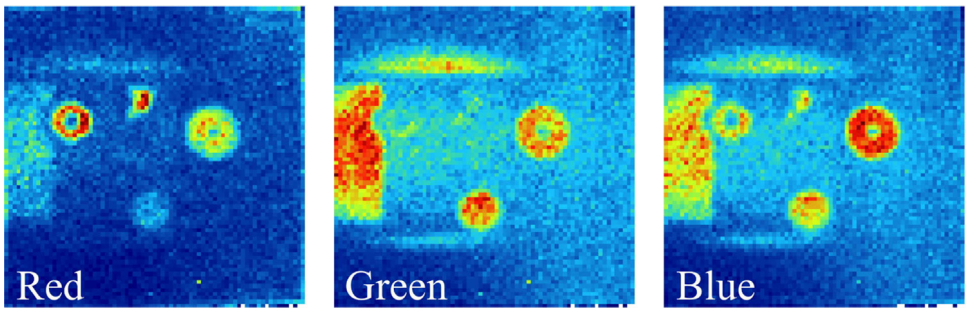

Fig. 15. Fluorescence mapping of a composite target in three adjacent energy bands [34].

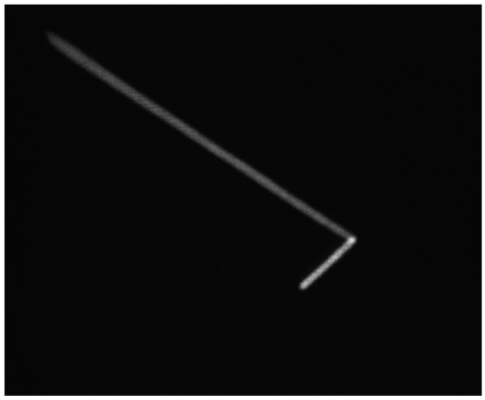

Fig. 16. A ^{220}Rn decay within the sensitive volume [34].

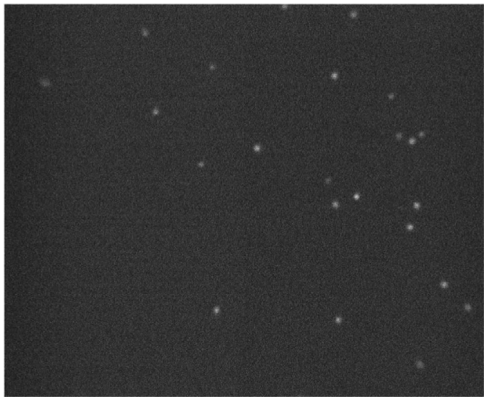

Fig. 17. 5.9 keV conversion X-rays [34].

It was found already in the eighties that some photosensitive vapors, added to the main gas constituents for applications in Cherenkov Ring Imaging, acted as effective internal wavelength shifters converting the main emission to lower frequencies easier to detect. Triethylamine (TEA) has a copious emission peaked at 280 nm in the region of transparency of thin polymer windows, permitting the optical recording of tracks with solid state cameras [29,30]; tetrakis dimethyl amino ethylene (TMAE) fluoresces at even longer wavelengths, peaked at 470 nm [31]. Fig. 11, from the quoted works, show an example of a cosmic particle interacting with the gas in the imaging chamber.

While very effective as scintillators, photosensitive vapors are rather inconvenient for use due to their reactivity. More recent work of several groups has found that carbon tetrafluoride, CF_4, originally studied in detectors owing to its small electron diffusion, under avalanche conditions has copious emission in the visible, around 650 nm, pure or in mixtures with noble gases [32,33]. Recorded with a triple-GEM detector suitable for optical recording (Fig. 12), Fig. 13 shows an integral image of neutron interactions in a ^{3}He-CF_4 mixture.

Fig. 14 shows schematically the optical imaging setup developed by CERN's Gas Detectors Development (GDD) group to perform energy-resolved fluorescence analysis. An X-ray tube is used to excite a target, and the soft X-ray fluorescence is imaged with a Triple-GEM chamber mounted as pinhole camera, recording position and energy of the detected photons. Selection of the events in three adjacent wavelength bands in the pulse height spectrum (named Red, Green and Blue) permits the identification of the materials in the composite target, Fig. 15 [34].

The multi-GEM device, with its voltage-controlled gain, permits to cover a wide range of applications, from the integrated fluorescence analysis illustrated above, to the detection of heavily ionizing tracks down to single photons (Fig. 16 and 17). Integration of the light emission results in an energy loss resolution comparable with the one obtained in the proportional charge gain mode.

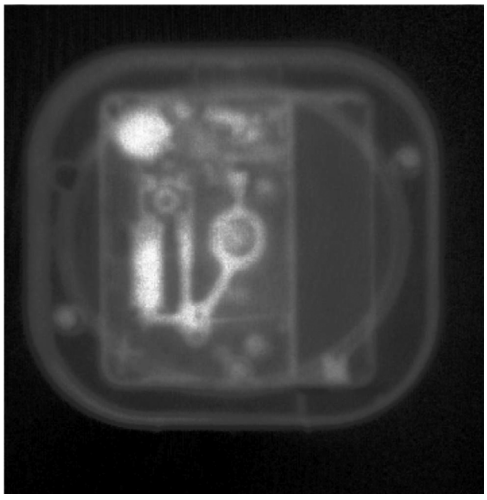

Fig. 18. X-ray optical radiography of a clock [35].

The glass GEM, with its large gains and rigid assembly, is particularly suitable for optical imaging [35]; Fig. 18 is an example of X-ray transmission radiography of a clock.

Large area (28×28 cm^2) glass plates have been operated with good energy resolution and gain uniformity [36]; the technology is particularly attractive for the development of sealed detectors, probably an essential requirement in view of commercial applications.

The very high rate capability of GEM devices is exploited in the optical imaging system developed for dose monitoring in hadrotherapy, shown in Fig. 19: while the detector is radiation-hard, the sensor has to be removed from the direct beam exposure with the help of a mirror [37]. Fig. 20 is an example of beam profile recorded with the

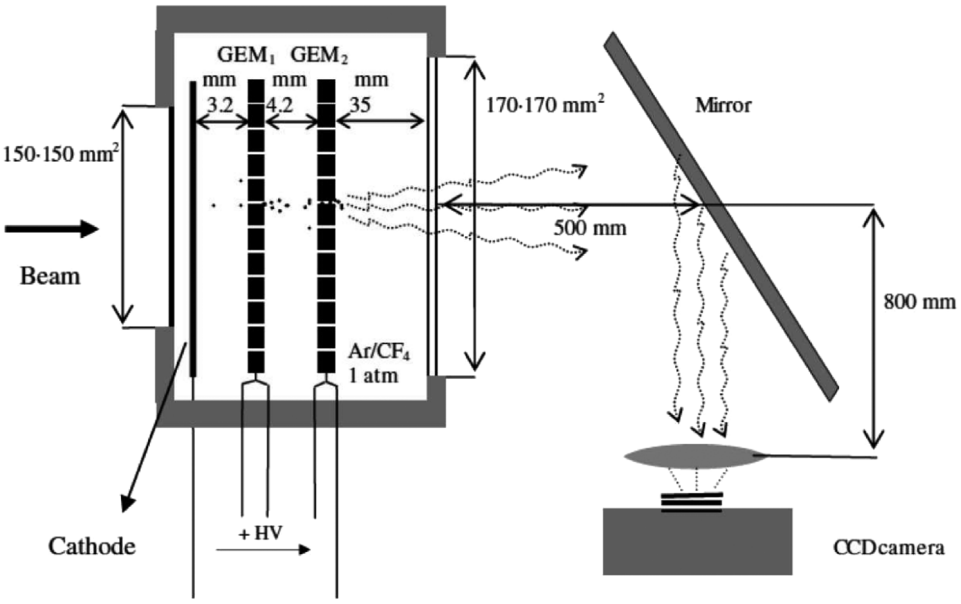

Fig. 19. Optical GEM for beam diagnostics and dose monitoring [37].

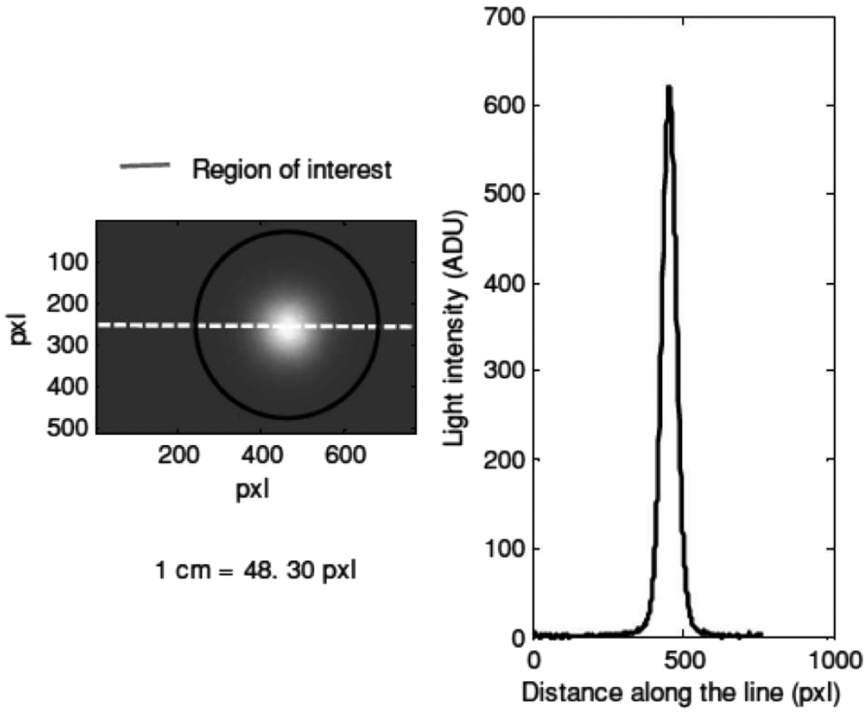

Fig. 20. Carbon beam profile recorded with the optical chamber. A CCD pixel is equivalent to an area in the detector of 207×207 μm^2 [37].

device. Named OptiGEM, an imaging tool based on this conception is commercially available [38].

4. Correction of the parallax error

In the imaging of neutral radiation, photons and neutrons, the thickness of the sensitive gas layer determines the efficiency of detection. While this does not affect the position determination for parallel beams, it introduces a parallax error that can largely deteriorate the localization accuracy for point-like sources or in pin-hole cameras.

The error can be corrected by the measurement of the time of conversion and taking into account the drift time of the ionization electrons. A method for the determination of coordinates exploiting the detection of primary scintillation in Xenon with a photomultiplier was devised long ago in the so-called Scintillating Drift Chamber [39]. The development of GEM devices with a CsI photosensitive layer permitted to record electronically both the prompt photoelectrons generated by the primary gas scintillation and the delayed and amplified ionization charge [40], thus in principle permitting the correction of parallax. So far however, only pure Xenon has been found to release enough primary photons to permit the detection of soft X-rays, limiting the extent of the applications.

An alternative solution is to build a detector having a radial electric field in the sensitive volume, coupled to the planar field of a

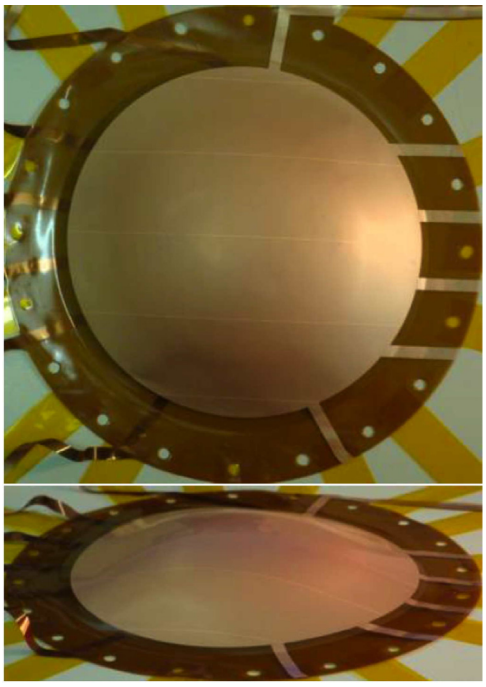

Fig. 21. The thermally shaped spherical GEM electrode during construction [42].

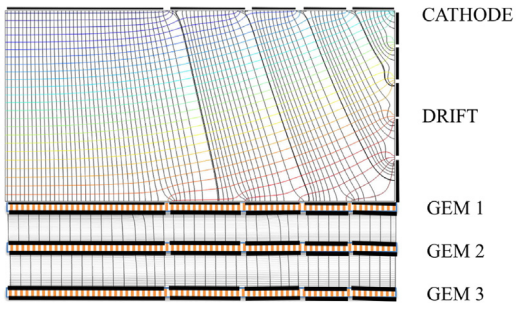

Fig. 22. Computed electric field in the Planispherical GEM detector [45].

position-sensitive detectors. Built along this principle, the Spherical Drift Chamber operated successfully for many year at LAL Orsay for imaging crystal diffraction patterns, but owing to the rather complex construction remained a one-of-the kind [41]. Recently, the GDD group at CERN has built and tested a "spherical" triple-GEM device, thermally shaping the electrodes after manufacturing of the holes; a patterned anode, also spherical in shape, mounts the readout electronics (Fig. 21 [42]).

Another way to solve the parallax error, described in the original GEM patent [43], is to pattern the cathode, GEM and anode with concentric rings, individually powered; a suitable choice of the potentials shapes the radial field and defines the focal length of the sensitive volume. The ionization electrons produced by X-ray conversions along a radius then drift to one or more amplification stages. Computed with the COMSOL software [44], Fig. 22 shows the equipotential and field lines for one half of a 10 cm diameter "Planispherical" GEM detector with a 10 cm focal length. A 3-D rendering of the device, currently in construction, is shown in Fig. 23 [45].

5. Conclusions and summary

The imaging applications briefly outlined in this note demonstrate the great flexibility of design and use of the present generation of

Fig. 23. The Planispherical GEM detector assembly, complete with the CCD camera holder [45].

the devices collectively named Micro-Pattern Gaseous Detectors. Fast and capable of high counting rates the new devices can be produced industrially in view of commercial applications in the fields of X-ray and neutron imaging, homeland security, elemental fluorescence analysis for archeology and cultural heritage and others. Positional information can be obtained from the collection of amplified charges with electronics systems, or with optical recording from the light emitted by fluorescence of the gases in the multiplication process.

References

[1] G. Charpak, et al., The use of multiwire proportional counters to select and localize charged particles, Nucl. Instrum. Methods 62 (1968) 262.
[2] G. Charpak, F. Sauli, High-resolution electronic particle detectors, Ann. Rev. Nucl. Part. Sci. 34 (1984) 285.
[3] F. Sauli, Applications of gaseous detectors in astrophysics, medicine and biology, Nucl. Instrum. Methods A323 (1992) 1.
[4] A. Oed, Position-sensitive detector With micro-strip anode for electron multiplication with gases, Nucl. Instrum. Methods A263 (1988) 351.
[5] F. Sauli, Development of high rate MSGCs: overview of results from RD-28, Nucl. Phys. B (Proc. Suppl.) 61B (1998) 236.
[6] B. Schmidt, Microstrip gas chambers: recent developments, radiation damage and long term behaviour, Nucl. Instrum. Methods A 419 (1998) 230.
[7] I. Giomataris, et al., Micromegas: a high-granularity, position-sensitive gaseous detector for high particle flux environments, Nucl. Instrum. Methods A376 (1996) 29.
[8] F. Sauli, GEM: a new concept for electron amplification in gas detectors, Nucl. Instrum. Methods A386 (1997) 531.
[9] J.M. Maia, et al., Advances in the micro-hole & strip plate gaseous detector, Nucl. Instrum. Methods A504 (2003) 364.
[10] A. Ochi, et al., Development of micro pixel chamber, Nucl. Instrum. Methods A478 (2002) 196.
[11] M. Titov, New developments and future perspectives of gaseous detectors, Nucl. Instrum. Methods A581 (2007) 25.
[12] D. Gonzalez-Diaz, High precision tracking and imaging with MPGDs, in: Proceedings of the Imaging 2016, Nucl. Instrum. Methods, Stokholm, 2016.
[13] S. Martou, et al., Development of the scalable readout system for micro-pattern gas detectors and other applications, J. Instrum. 8 (2013) C03015.
[14] A. Bressan, et al., Two-dimensional readout in GEM detectors, Nucl. Instrum. Methods A425 (1999) 254.
[15] T. Koike, et al., A new gamma-ray detector with gold-plated gas electron multiplier, Nucl. Instrum. Methods A 648 (2011) 180.
[16] M. Danielsson, et al., Novel gaseous detectors for medical imaging, Nucl. Instrum. Methods A518 (2004) 406.
[17] J. Östling, et al., A radiation-tolerant electronic readout system for portal imaging, Nucl. Instrum. Methods A 525 (2004) 308.
[18] <http://c-rad.se/product/gemini/>.
[19] M. Klein, C.J. Schmidt, CASCADE, neutron detectors for highest count rates in combination with ASIC/FPGA based readout electronics, Nucl. Instrum. Methods A 628 (2011) 9.
[20] G. Croci, et al., GEM-based thermal neutron beam monitors for spallation sources, Nucl. Instrum. Methods A732 (2013) 217.
[21] A.L.M. Silva, et al., Performance of a gaseous detector based energy dispersive X-ray fluorescence imaging system: analysis of human teeth treated with dental amalgam, Spectrochim. Acta B86 (2013) 115.
[22] A.L.M. Silva, et al., A large area full-field EDXRF imaging system based on a THCOBRA gaseous detector, J. Anal. At. Spectrom. 30 (2015) 345.
[23] R. Bellazzini, et al., Reading a GEM with a VLSI pixel ASIC used as direct charge collecting anode, Nucl. Instrum. Methods A 535 (2004) 477.

[24] H.F.H. Li, et al., Assembly and test of the gas pixel detector for X-ray polarimetry, Nucl. Instrum. Methods A804 (2015) 155.
[25] M. Campbell, X-ray imaging and single particle detection using the Medipix chip family, in: Proceedings of the Imaging 2016, Nucl. Instrum. Methods, Stokholm, 2016.
[26] S.P. George, et al., Particle tracking with a timepix based triple GEM detector, J. Instrum. 10 (2015) P11003.
[27] D. Pacella, et al., An hybrid detector GEM-ASIC for 2-D soft X-ray imaging for laser produced plasma and pulsed sources, J. Instrum. 11 (2016) C03022.
[28] H. van der Graaf, et al., Recent GridPix results: an integrated micromegas grid and an ageing test of a micromegas chamber, Nucl. Instrum. Methods A566 (2006) 62.
[29] M. Suzuki, et al., The emission spectra of Ar, Kr and Xe + tea, Nucl. Instrum. Methods A254 (1987) 556.
[30] G. Charpak, et al., An optical, proportional, continuously operating avalanche chamber, Nucl. Instrum. Methods A258 (1987) 177.
[31] A. Breskin, et al., A high efficiency low-pressure UV-rich detector with optical avalanche recording, Nucl. Instrum. Methods A273 (1988) 798.
[32] F.A.F. Fraga, et al., CCD readout of GEM-based neutron detectors, Nucl. Instrum. Methods A478 (2002) 357.
[33] A. Morozov, et al., Effect of electric field on the primary scintillation from CF4, Nucl. Instrum. Methods A628 (2011) 360.
[34] A. Beschi, et al., Construction and operation of a multipurpose GEM detector with an optical readout, Subm. Nucl. Instrum. Methods (2016).
[35] H. Takahashi, et al., Development of a glass GEM, Nucl. Instrum. Methods A724 (2013) 1.
[36] Y. Mitsuya, et al., Developmant of large-area glass GEM, Nucl. Instrum. Methods A795 (2015) 156.
[37] E. Seravalli, et al., 2D dosimetry in a proton beam with a scintillating GEM detector, Phys. Med. Biol. 54 (2009) 3755.
[38] <http://www.phenixmedical.com> .
[39] G. Charpak, et al., The scintillating drift chamber: a new tool for high-accuracy, very high-rate particle localzation, Nucl. Instrum. Methods 126 (1975) 381.
[40] T. Meinschad, et al., Detection of primary and field-enhanced scintillation in xenon with a CsI-coated GEM detector, Nucl. Instrum. Methods A547 (2005) 342.
[41] G. Charpak, et al., The spherical drift chamber for x-ray imaging applications, Nucl. Instrum. Methods 122 (1974) 307–312.
[42] S. Duarte Pinto, et al., First results of spherical GEMs, in: Proceedings of the IEEE Nuclear Science Symposium Conference Records, Knoxville, 2011.
[43] F. Sauli, Radiation Detector of very high performance and Planispherical Parallax-Free X-Ray Imager (Editor), CERN, 1999.
[44] <https://www.comsol.com> .
[45] F. Brunbauer, et al., The planispherical chamber: a parallax-free X-ray gaseous detector for imaging applications, Subm. Nucl. Instrum. Methods (2016).